# Optical transitions involving unconfined energy states in $In_xGa_{1-x}As/GaAs$ multiple quantum wells

G. Ji, W. Dobbelaere, D. Huang, and H. Morkoç
*Coordinated Science Laboratory, University of Illinois at Urbana-Champaign, 1101 West Springfield Avenue, Urbana, Illinois 61801-3082*
(Received 30 November 1987; revised manuscript received 26 September 1988)

Optical transitions with energies higher than that of the GaAs band gap in highly strained $In_xGa_{1-x}As/GaAs$ multiple-quantum-well structures have been observed in photoreflectance spectra. In some samples as many as seven such structures were present. We identify them as transitions between the unconfined electron states and the confined heavy-hole states. For energies below the GaAs signal, intense transitions corresponding to such unconfined electron subbands were also observed. The intensity of the transitions involving unconfined electron subbands decreases with increasing well width, but is weakly dependent on the mole fraction $x$. The transmission coefficients are calculated in order to locate the positions of the unconfined electron subband energies. Good agreement is obtained between the experimental data and the theoretical calculation.

## I. INTRODUCTION

In quantum-well structures the quantized electron states confined in the quantum-well region have been extensively studied. But transitions from the unconfined states have not yet received as much attention. Unconfined transitions have already been observed in $Al_xGa_{1-x}As/GaAs$ multiple-quantum-well structures (MQWS).[1-3] The intensity of the transition involving the first unconfined conduction-band states and the first heavy-hole valence states was reported to depend strongly on the barrier width.[2] The energies of the transitions involving the unconfined states can be predicted by a two-band tight-binding model,[4,5] with good agreement resulting between experiments and theory.

Recently, advances in crystal-growth techniques have allowed the extension of $Al_xGa_{1-x}As/GaAs$ superlattices to the lattice-mismatched materials such as $In_xGa_{1-x}As/GaAs$,[6,7] $GaAs_{1-y}P_y/GaAs$,[8] and $GaAs_{1-y}Sb_y/GaAs$.[9,10] The remarkable progress in modulation-doped field-effect transistors using $In_xGa_{1-x}As/GaAs$ heterostructures has brought a great deal of attention to the $In_xGa_{1-x}As/GaAs$ system.[11] The band structure of $In_xGa_{1-x}As/GaAs$ has been investigated by various optical techniques such as photoluminescence,[12,13] transmission spectroscopy,[14] and photoreflectance (PR).[15] PR technique is preferred in many cases because of its simplicity and ability to provide detailed information at room temperature. Besides PR has the additional advantage in that it has better sensitivity than other optical measurements, particularly for higher-order transitions. Both allowed and symmetry forbidden transitions can be observed.[13,16] All of these encourage one to use this valuable technique for a detailed investigation of such an important $In_xGa_{1-x}As/GaAs$ material system.

In this study we report the observation of the PR signal with energy higher than that of the GaAs barrier. These features are attributed to the transitions between the unconfined conduction subbands and the confined valence subband in $In_xGa_{1-x}As/GaAs$ MQWS. As many as seven transitions above the GaAs signal were observed and have been assigned to unconfined states. Some transitions with energies less than the GaAs energy gap are also identified as being due to unconfined states. Good agreement between theoretical calculations and measurements confirms our identification and also proves that the calculation of the transmission coefficient which is what we utilized, is an effective way to predict the positions of the unconfined states.

## II. EXPERIMENTAL DETAILS

The samples studied were grown by molecular-beam epitaxy on a Si-doped GaAs substrate. We have grown two sets of $In_xGa_{1-x}As/GaAs$ samples. Group A has two samples, 1 and 2, which have the different well widths (42 and 81 Å) but the same barrier width (200 Å) and high InAs mole fractions ($\sim 0.25$). Group B has three samples 3, 4, and 5, which also have the different well widths (85, 159, and 213 Å) and the same barrier width (200 Å) and low InAs mole fraction ($x = 0.15$). (We call the $In_{1-x}Ga_xAs$ layer as well and the GaAs layer barriers, which is only for electron and heavy hole, but not light hole.) The sample parameters were listed in Table I. The low-temperature optical transmission spectra for group B were reported in our previous study.[17]

The PR spectra were measured at room temperature (300 K). The experimental arrangement of the PR technique was discussed in detail by Shay,[18] and therefore, will not be repeated here. In our experiment, a 1-mW HeNe laser, mechanically chopped at 90 Hz, was used to modulate the optical constants of the MQW's structures. The reflected light was detected by an EG&G type HUV-1100 (BG)-Si photodiode. The intensity of the laser pump beam, the probe beam, and the recording system

 

TABLE I. The comparison of the PR measurements with numerical calculations at $T=300$ K (where Id. denotes identification).

| Sample | | 1 | | | 2 | | | 3 | | | 4 | | | 5 | |
|---|---|---|---|---|---|---|---|---|---|---|---|---|---|---|---|
| $x$ | | 0.256 | | | 0.236 | | | 0.155 | | | 0.146 | | | 0.151 | |
| $L_w$ (Å) | | 42 | | | 81 | | | 85 | | | 159 | | | 213 | |
| $L_b$ (Å) | | 200 | | | 200 | | | 200 | | | 200 | | | 200 | |
| | Expt. | Cal. | Id. | Expt. | Cal. | Id. | Expt. | Cal. | Id. | Expt. | Cal. | Id. | Expt. | Cal. | Id. |
| Transitions | 1.262 | 1.258 | 1*C*-1*H* | 1.222 | 1.219 | 1*C*-1*H* | 1.287 | 1.290 | 1*C*-1*H* | 1.277 | 1.279 | 1*C*-1*H* | 1.276 | 1.271 | 1*C*-1*H* |
| between | 1.306 | 1.299 | 1*C*-2*H* | 1.249 | 1.253 | 1*C*-3*H* | 1.321 | 1.318 | 1*C*-3*H* | 1.295 | 1.292 | 1*C*-3*H* | 1.302 | 1.303 | 2*C*-2*H* |
| confined | 1.329 | 1.330 | 1*C*-1*L* | 1.292 | 1.295 | 1*C*-1*L* | 1.350 | 1.346 | 1*C*-1*L* | 1.318 | 1.326 | 2*C*-2*H* | 1.330 | 1.325 | 1*C*-1*L* |
| states | | | | 1.337 | 1.338 | 2*C*-2*H* | 1.383 | 1.379 | 2*C*-2*H* | 1.325 | 1.332 | 1*C*-1*L* | 1.348 | 1.351 | 3*C*-3*H* |
| | | | | | | | | | | 1.382 | 1.384 | 3*C*-3*H* | | | |
| Transitions | 1.371 | 1.377 | 2*C*-1*H* | 1.384 | 1.375 | 3*C*-1*H* | 1.480 | 1.465 | 5*C*-3*H* | 1.433 | 1.440 | 6*C*-1*H* | 1.385 | 1.390 | 4*C*-1*H* |
| involving | 1.442 | 1.451 | 3*C*-2*H* | | 1.392 | 3*C*-2*H* | 1.493 | 1.500 | 6*C*-1*H* | 1.465 | 1.454 | 6*C*-3*H* | 1.433 | 1.430 | 5*C*-5*H* |
| unconfined | 1.467 | 1.460 | 4*C*-2*H* | 1.445 | 1.433 | 4*C*-2*H* | 1.512 | 1.511 | 6*C*-2*H* | | 1.465 | 6*C*-4*H* | 1.459 | 1.452 | 7*C*-3*H* |
| conduction | | 1.465 | 5*C*-1*H* | | 1.455 | 4*C*-3*H* | 1.540 | 1.528 | 6*C*-3*H* | | | | | 1.461 | 7*C*-4*H* |
| subbands | 1.485 | 1.489 | 6*C*-1*H* | 1.478 | 1.478 | 4*C*-4*H* | 1.564 | 1.566 | 7*C*-1*H* | | | | | | |
| | 1.508 | 1.506 | 5*C*-2*H* | | 1.482 | 5*C*-1*H* | | | | | | | | | |
| | 1.529 | 1.530 | 6*C*-2*H* | 1.495 | 1.495 | 5*C*-2*H* | | | | | | | | | |
| | 1.568 | 1.543 | 7*C*-1*H* | 1.522 | 1.516 | 5*C*-3*H* | | | | | | | | | |
| | | 1.584 | 7*C*-2*H* | 1.542 | 1.543 | 5*C*-4*H* | | | | | | | | | |
| | | | | | 1.543 | 6*C*-1*H* | | | | | | | | | |
| | | | | 1.567 | 1.557 | 6*C*-2*H* | | | | | | | | | |
| | | | | | 1.578 | 6*C*-3*H* | | | | | | | | | |
| | | | | 1.597 | 1.604 | 6*C*-4*H* | | | | | | | | | |

were set at the same condition when measuring the different samples for a qualitative comparison of the intensity of PR signals.

## III. THEORETICAL CONSIDERATION

$In_xGa_{1-x}As$ layers, grown on a GaAs buffer, sustain biaxial in-plane compression and corresponding along the ⟨001⟩ growth direction. For samples with small InAs mole fraction, $x$, and with relatively small $In_xGa_{1-x}As$ layer thickness, the lattice mismatch between the $In_xGa_{1-x}As$ and GaAs layers is believed to be entirely accommodated by the tegtragonal elastic deformation of the $In_xGa_{1-x}As$ layers. The band structure including strain effects should be considered in calculating the subband energies, for both confined and unconfined electron states. As shown in our previous study the strain dependent Kane's eight-band $\mathbf{k}\cdot\mathbf{p}$ model is sufficient to describe the subband transitions.[17] Interested readers may refer to the work of Pötz *et al.*[19,20] for a generalization of Kane's eight-band $\mathbf{k}\cdot\mathbf{p}$ model including remote-band effects, band nonparabolicity, and strain effects in the second-order perturbation theory.

To determine the subband structure, we first calculated the energies for confined states. The details of the calculation can be found in our previous work.[17] The material parameters used in this study can be found in Table I of Ref. 17. For the $In_xGa_{1-x}As/GaAs$ system the valence-band discontinuity (for heavy hole) is taken to be 30% from our previous study using the optical transmission (4 K) studies.[17] The unstrained band gap of bulk $In_xGa_{1-x}As$ is used as an input parameter to calculate the $In_xGa_{1-x}As/GaAs$ subband energies. Only the $\Gamma$ band is considered.

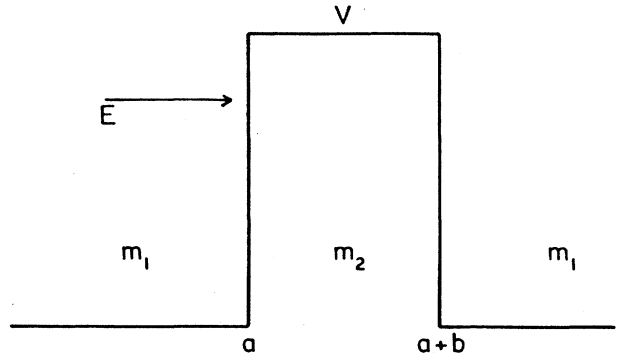


FIG. 1. Rectangular barrier between $x=a$ and $x=a+b$, with barrier height $V$. A particle having energy $E$ is injected from left, partially reflected and partially passed. The effective mass is $m_1$ outside the barrier and $m_2$ inside the barrier.

The unconfined electron subband energies are determined by the calculation of the transmission coefficient. We first consider a rectangular barrier between $x=a$ and $x=a+b$ with height $V$ as shown in Fig. 1. This treatment is then extended to account for multiple barriers. In different regions the effective masses are assumed to be different as $m_1$ and $m_2$, respectively. The solutions of the Schrödinger equation in the three regions are given as

$$\varphi(x)=\begin{cases}\psi_{\rm I}(x)=Ae^{ikx}+Be^{-ikx}, & m=m_1 \quad \text{for } x\le a & \text{(1a)}\\ \psi_{\rm II}(x)=Ce^{-iqx}+De^{iqx}, & m=m_2 \quad \text{for } a\le x\le b+a & \text{(1b)}\\ \psi_{\rm III}(x)=Fe^{ikx}+Ge^{-ikx}, & m=m_1 \quad \text{for } x\ge a+b\ , & \text{(1c)}\end{cases}$$

where

$$k=\left[\frac{2m_1E}{\hbar^2}\right]^{1/2}$$

and

$$q=\left[\frac{2m_2(E-V)}{\hbar^2}\right]^{1/2}.$$

The wave function and particle current density should be continuous across the interface at $x=a$ and $x=a+b$, i.e.,

$$\psi_{\rm I}(a)=\psi_{\rm II}(a)\ ,$$
$$\frac{1}{m_1}\frac{d\psi_{\rm I}}{dx}\bigg|_{x=a}=\frac{1}{m_2}\frac{d\psi_{\rm II}}{dx}\bigg|_{x=a}\ , \qquad \text{(2a)}$$
$$\psi_{\rm II}(a+b)=\psi_{\rm III}(a+b)\ ,$$
$$\frac{1}{m_2}\frac{d\psi_{\rm II}}{dx}\bigg|_{x=a+b}=\frac{1}{m_1}\frac{d\psi_{\rm III}}{dx}\bigg|_{x=a+b}\ . \qquad \text{(2b)}$$

From Eqs. (1) and (2), we obtain

$$\begin{bmatrix}A\\B\end{bmatrix}=\underline{M}\begin{bmatrix}F\\G\end{bmatrix}\ , \qquad \text{(3a)}$$

where

$$\underline{M}=\begin{bmatrix}\left[\cos(qb)-i\frac{\varepsilon}{2}\sin(qb)\right]e^{ikb} & -\frac{i\eta}{2}\sin(qb)e^{-ik(b+2a)}\\ \frac{i\eta}{2}\sin(qb)e^{ik(b+2a)} & \left[\cos(qb)+i\frac{\varepsilon}{2}\sin(qb)\right]e^{-ikb}\end{bmatrix} \qquad \text{(3b)}$$

and

$$\varepsilon=\frac{q}{k}\frac{m_1}{m_2}+\frac{k}{q}\frac{m_2}{m_1},$$

$$\eta=\frac{q}{k}\frac{m_1}{m_2}-\frac{k}{q}\frac{m_2}{m_1}.$$

The transmission coefficient $T$ is given by

$$T=\left[\frac{F}{A}\right]^2=\frac{1}{|M_{11}|^2}. \tag{4}$$

For a potential with arbitrary shape the total potential is divided into a series of rectangular barriers. The above-mentioned method is extended to the case of multiple barriers. For the $i$th barrier having a barrier height $V_i$, effective mass $m_i$, and width $b_i$, a transform matrix $\underline{M}_i$ is obtained from Eq. (3b). The final transform matrix $\underline{M}=\prod_i \underline{M}_i$ and the final transmission coefficient $T$ can be obtained from Eq. (4).

In order to obtain the transition energies between subbands from the PR spectra, the third-derivative functional form (TDFF) (Ref. 21) was used to fit experimental results:

$$\frac{\Delta R}{R}=\mathrm{Re}\left[\sum_{j=1}^{p} C_j e^{i\Phi_j}(E-E_{gj}+i\Gamma_j)^{-m_j}\right], \tag{5}$$

where $C_j$, $\Phi_j$, $E_{gj}$, and $\Gamma_j$ are the amplitude, phase, transition energy, and broadening parameter of the $j$th structure, respectively. In this study we did not attempt to analyze the PR line shape. Although many results have been published with regard to the PR line shape,[22–24] the details are still remaining to be understood. The main problem is that the mechanism of PR, i.e., how the band structure of a quantum well is modulated by the incident laser, is still not well understood. Thus, all of the fitting procedure, either first derivative or third derivative are only phenomenological. This situation becomes worse by the observed interference effects originating from substrate-barrier-cap layer in PR spectra as reported by Zheng *et al.*[25] However, as being demonstrated by Shanabrook *et al.*[22] and Pan *et al.*,[26] first- and third-derivative functional forms yield a comparable fit. The energy positions of the various spectral features are relatively insensitive to the particularly derivative form of the line-shape fit. In addition, the three-dimensional (3D) properties (large dispersion in growth direction) of the unconfined electron subbands distinquish them from the confined states. For above reasons, we believe that the energies obtained from the fitting of the TDFF should be appropriate at least for the energies associated with unconfined electron subbands.[22]

## IV. RESULTS AND DISCUSSION

In Fig. 2, we present the PR spectra for samples 1 and 2. The solid arrows indicate the transition energies obtained from the theoretical calculation as discussed in the preceding section. The dashed arrows give the observed energies derived from the fitting of TDFF [Eq. (5)] to the experimentally recorded PR spectra. The assignments of the various transitions are based on the energy comparison between the theory and experiment, where *nC-mH* (*nC-mL*) denotes the transition between *n*th conduction subband and *m*th heavy- (light-) hole valence subband. In addition to the PR signal from the MQWS, a strong feature corresponding to the GaAs band gap, presumably due to the GaAs buffer, is also observable. Obviously, the features with energies higher than the GaAs band gap should be associated with subbands having energies higher than the barrier, which are known as the unconfined states.

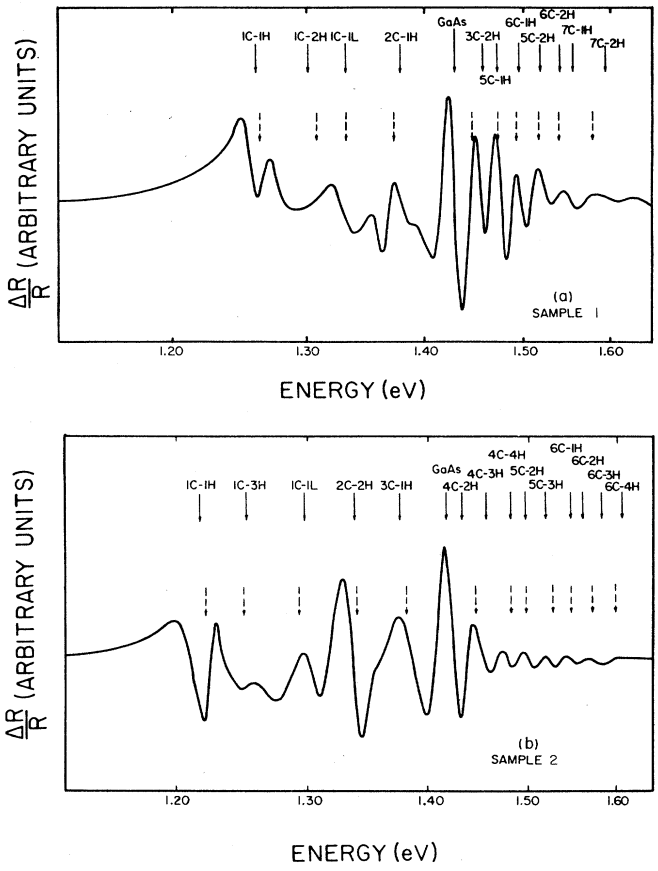


FIG. 2. PR spectra for $In_xGa_{1-x}As/GaAs$ MWQS at $T=300$ K: (a) sample 1, $L_w=42$ Å, $L_B=200$ Å, $x=0.256$; (b) sample 2, $L_w=81$ Å, $L_B=200$ Å, $x=0.236$. The solid arrows indicate the transition energies obtained from the theoretical calculation as discussed in the text. The dashed arrows give the observed energies derived from the fitting of TDFF [Eq. (5)] to the experimentally recorded PR spectra.

It is well known that the excitonic resonance is dominant in optical absorption even at room temperature for type-I MQWS due to the confinement of electrons and holes in the same space layer. The excitonic transition are also very important in PR spectra as well. However for type-II MQWS, such as the light hole in the $In_xGa_{1-x}As/GaAs$ system, the electrons and light holes are confined in different space layers. Thus, the excitonic absorption is no longer important due to the relatively

large electron-hole separation, and possible interfacial imperfections. For unconfined states, the electrons (or holes) are no longer two dimensional and associated wave functions are extended, or 3D-like. Similar to bulk GaAs at room temperature, we expect that for the transitions associated with unconfined states the excitonic effect will not be important. Based on the above arguments, the exciton binding energy $E_b$ was included in our calculations for the electron–heavy-hole transitions between confined electron subbands. The value of $E_b$ was estimated to be about 8 meV for the samples used in this study. For the transitions associated with light holes or unconfined states, the band-to-band transition was assumed.

The energies of the unconfined states were determined from the calculation of the transmission coefficients as described in the preceding section. In fact, the subbands are the resonant states which appear in the calculated transmission spectra. Figure 3 presents the results of the transmission spectra for electrons in samples 1 and 2. The parameters for the $In_xGa_{1-x}As$ and GaAs layers are used in calculation. The energy zero corresponds to the bottom of the quantum well (or $In_xGa_{1-x}As$ layer). The threshold energy ( $\sim$200 meV), above which the transmission increases rapidly, corresponds to the top of barrier (or GaAs layer). As one can see, the spectra show clearly the resonance peak at energies above the barriers. The peak energies represent the location of possible unconfined conduction subbands. The width of each peak, $\Delta E$, and the average lifetime $\Delta\tau$ of electrons staying at such resonant states are related by the uncertainty relation $\Delta E \Delta\tau \sim \hbar$. It should be noted that the confined

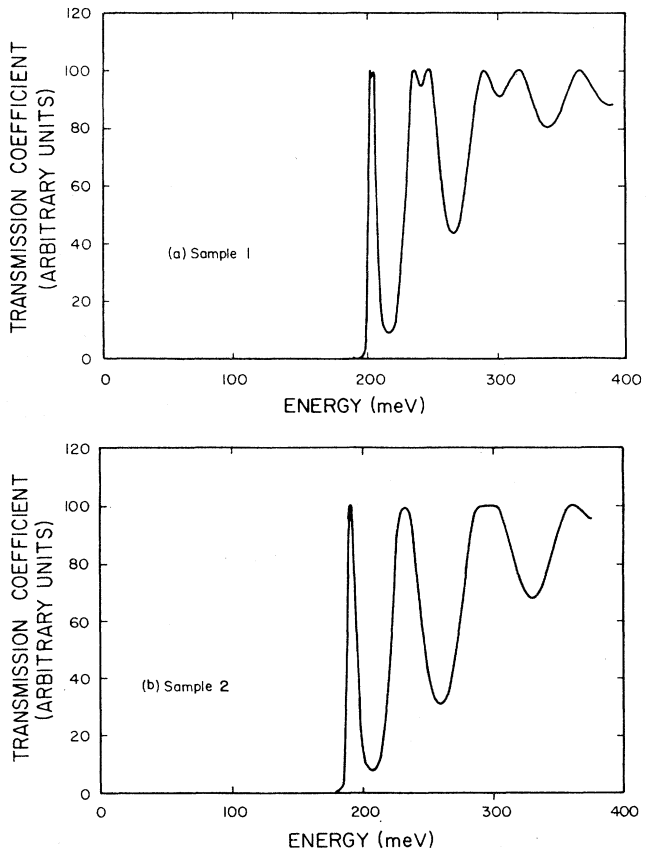


FIG. 3. The transmission coefficients vs energies calculated from Eqs. (1)–(4) for $In_xGa_{1-x}As/GaAs$ MQW's samples: (a) sample 1, $L_w=42$ Å, $L_B=200$ Å, $x=0.256$; (b) sample 2, $L_w=81$ Å, $L_B=200$ Å, $x=0.236$.

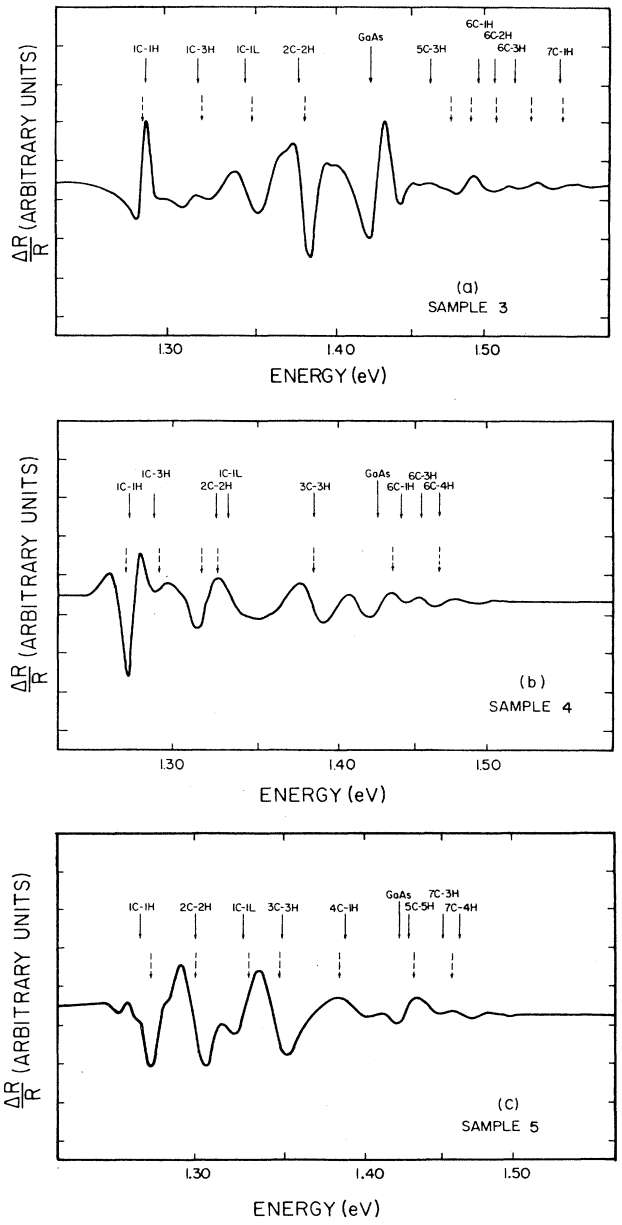


FIG. 4. PR spectra for $In_xGa_{1-x}As/GaAs$ MQWS at $T=300$ K: (a) sample 3, $L_w=85$ Å, $L_B=200$ Å, $x=0.155$; (b) sample 4, $L_w=159$ Å, $L_B=200$ Å, $x=0.146$; (c) sample 5, $L_w=213$ Å, $L_B=200$ Å, $x=0.151$. The solid arrows indicate the transition energies obtained from the theoretical calculation as discussed in the text. The dashed arrows give the observed energies derived from the fitting of TDFF [Eq. (5)] to the experimentally recorded PR spectra.

electron subbands can also be found via the calculation of the transmission spectra, in principle, since they are also the resonant states. However, for the quantum well with large ($\geq 100$ Å) barrier thickness, the transmission coefficient is much too small to be shown on Fig. 3 with the same scale.

The comparison between the calculations and measurements is given in Table I for all of the five samples studied. The calculated energies of the confined electron subbands are obtained from the three-band Kane's model including strain effects.[27] The energies of the unconfined conduction subbands are obtained from the calculation of the transmission coefficients using Eqs. (1)–(4). The measured transition energies between the different electron subbands were determined by fitting Eq. (5) to the observed PR spectra. As one can see, the overall agreement between the measured data and calculations is quite good. The deviations for most of the transitions are several meV's which is within the uncertainty in determining the energies in PR spectra. For clarity, we also give the PR spectra for samples 3, 4 and 5 in Figs. 4(a), 4(b), and 4(c), respectively, with the observed and calculated transition energies indicated.

The transitions with energies above the GaAs barrier should involve unconfined electron subbands. However, as we found, the transitions with energies below the GaAs barrier can also involve unconfined subbands. The feature, $2C$-$1H$, at energy 1.371 eV in Fig. 2(a) for sample 1 is one of the transitions associated with the second conduction subband which is unconfined. Sample 1 has a well thickness of 42 Å and InAs mole fraction of 25.6%. Only the first conduction subband is confined in this sample. Similar transitions were observed in samples 2 and 5, as well.

The selection rule for optical transitions between electron subbands deeply confined in quantum wells is no longer applicable for those associated with unconfined states.[2,26] There is no longer a simple relationship between the number of nodes in the wave function in the well and the energy of the state. Additional nodes may appear in the barrier due to the large leakage of the wave function into the barrier. Thus the parity of the states, with respect to the center of the well, is no longer alternate.[2] In order to obtain the transition intensity, a detailed calculation of matrix elements must be performed. Both the tight-binding and envelope-function models are applicable.

It can be noticed from Figs. 2 and 4 that the narrow wells lead to stronger unconfined transitions, and such transitions are very weak when the well width is wider than 200 Å. The mole fraction $x$ has only a little effect on the intensity of such PR signals. Very strong signals have been observed in sample 1 with a well width $L_w = 42$ Å and $x = 0.256$. A monotonic decrease of unconfined transitions is seen as the quantum well thickness is increased from $L_w = 42$ to 200 Å. This can be explained qualitatively as follows: First, the wave function of unconfined conduction bands must be located around the well region. For a narrow well, the overlap between the wave functions of conduction and hole states must be large causing a strong PR signal. Second, the PR signal is proportional to $k_z$, the cutoff of Brillouin zone in the $z$ direction,[21] $k_z \sim 1/L_w$ is larger for a MQW with a narrow well width, and so is the PR signal. Third, when the well width becomes wider, the signal from the different heavy-hole subbands and the same unconfined conduction states overlap. This introduces extra cancellation between the neighboring signals. A quantitative comparison is difficult to make since the sample quality might change from sample to sample.

In conclusion, we have observed a series of transitions involving unconfined conduction subbands and the confined heavy- (light-) hole subbands in highly strained $In_xGa_{1-x}As/GaAs$ MQW's with quantum-well thickness, between, 42 and 200 Å, $x = 0.15-0.26$. The intensity of these unconfined transitions depends strongly on the well width $L_w$, but weakly on the mole fraction $x$. The transmission coefficients have been calculated in order to determine the energies of these unconfined states. Good agreement has been obtained between the calculations and PR measurements. We believe that the transitions involving the unconfined states are band-to-band transition, and do not involve excitons.

## ACKNOWLEDGMENTS

This research is supported by U.S. Air Force Office of Scientific Research (AFOSR), by U.S. National Aeronautics and Space Administration (NASA), by National Science Foundation (Materials Research Laboratory Program), and by U.S. Department of Energy (under Contract No. DE-AC02-76ER01198). The authors would like to acknowledge fruitful discussions with Professor F. H. Pollak and Dr. C. W. Litton. Mr. Dobbelaere would like to thank the Belgian-American Educational Foundation for partial support.

[1] J. J. Song, Y. S. Yoon, P. S. Jung, A Fedotowsky, J. N. Schulman, C. W. Tu, J. M. Brown, D. Huang, and H. Morkoç, Appl. Phys. Lett. **50**, 1269 (1987).

[2] J. J. Song, Y. S. Yoon, A. Fedotowsky, Y. B. Kim, J. N. Schulman, C. W. Tu, D. Huang, and H. Morkoç, Phys. Rev. B **34**, 8958 (1986).

[3] U. K. Reddy, G. Ji, T. Henderson, H. Morkoç, and J. N. Schulman, J. Appl. Phys. **62**, 145 (1987).

[4] G. A. Sia-Halasz, L. Esaki, and W. A. Harrison, Phys. Rev. B **18**, 2812 (1972).

[5] J. N. Schulman, Proc. Mater. Res. Soc. **56**, 279 (1986).

[6] J. Y. Marzin and E. V. K. Rao, Appl. Phys. Lett. **43**, 560 (1983).

[7] I. J. Fritz, L. R. Dawson, and T. E. Zipperian, J. Vac. Sci. Technol. B **1**, 387 (1983).

[8] G. C. Osbourn, J. Appl. Phys. **53**, 1586 (1982).

[9] C. J. Nuese, IEEE Int. Electron. Dev. Technol. Dig. **76**, 125 (1976).

[10] G. B. Stringfellow, J. Electron. Mater. **10**, 919 (1981).

[11] T. Henderson, M. I. Aksan, C. K. Peng, H. Morkoç, P. C.

Chao, P. M. Smith, K.-H. Duh, and L. F. Lester, IEEE Electron. Dev. Lett. **EDL-7**, 649 (1986).

[12]A. P. Roth, R. A. Masut, M. Sacilotti, P. J. D'Arcy, Y. Lepage, G. J. Sproule, and D. F. Mitchell, Superlatt. Microstruct. **2**, 507 (1986).

[13]N. G. Anderson, W. D. Laidig, R. M. Kolbas, and Y. C. Lo, J. Appl. Phys. **60**, 2361 (1986).

[14]J. Y. Marzin, M. N. Charasse, and B. Sermage, Phys. Dev. B **31**, 8298 (1985).

[15]U. K. Reddy, G. Ji, T. Henderson, D. Huang, R. Houdré, H. Morkoç, and C. W. Litton (unpublished).

[16]H. Shen, P. Parayanthal, F. H. Pollak, A. L. Smirl, J. N. Schulman, R. A. McFarlane, and I. D'Haenens, in *Proceedings of the 18th International Conference on the Physics of Semiconductors, Stockholm, Sweden, 1986,* edited by O. Engström (World Scientific, Singapore, 1986), p. 561.

[17]G. Ji, D. Huang, U. K. Reddy, T. S. Henderson, R. Hondré, and H. Morkoç, J. Appl. Phys. **62**, 3366 (1987).

[18]J. L. Shay, Phys. Rev. B **2**, 803 (1970).

[19]W. Pötz, W. Porod, and D. K. Ferry, Phys. Rev. B **32**, 3868 (1985).

[20]W. Pötz and D. K. Ferry, Superlatt. Microstruct. **2**, 151 (1986).

[21]D. E. Aspens, in *Handbook on Semiconductors,* edited by T. S. Moss (North-Holland, New York, 1980), Vol. 2, p. 109.

[22]B. V. Shanabrook, O. J. Glembocki, and W. T. Beard, Phys. Rev. B **35**, 2540 (1987).

[23]Y. Tang, B. Wang, D. Jiang, W. Zhuang, and J. Liang, Solid State Commun. **63**, 793 (1987).

[24]W. M. Theis, G. D. Sanders, C. E. Leak, K. K. Bajaj, and H. Morkoç, Phys. Rev. B **37**, 3042 (1988).

[25]X. L. Zheng, D. Herman, B. Lax, and F. H. Chambers, Appl. Phys. Lett. **52**, 287 (1988).

[26]S. H. Pan, H. Shen, Z. Hang, F. H. Pollak, W. Zhuang, Q. Xu, A. P. Roth, R. Masut, C. LeCelle, and D. Morris, Phys. Rev. B **38**, 3375 (1988).

[27]J. Y. Marzin, in *Heterojunctions and Semiconductor Superlattices,* edited by G. Allan, G. Bastand, N. Boccara, M. Lannoo, and M. Voos (Springer, Berlin, 1986), p. 161.